

# Probing the growth of supermassive black holes at $z > 6$ with LOFAR

Kirsty J. Rhook<sup>1\*</sup> & Martin G. Haehnelt<sup>1,2†</sup>

<sup>1</sup>*Institute of Astronomy, Madingley Road, Cambridge CB3 0HA*

<sup>2</sup>*Kavli Institute for Theoretical Physics, Kohn Hall, UCSB, Santa Barbara CA 93106*

August 29th, 2006

## ABSTRACT

HII regions surrounding supermassive black holes (BHs) in an otherwise still neutral intergalactic medium (IGM) are likely to be the most easily detectable sources by future 21cm experiments like LOFAR. We have made predictions for the size distribution of such HII regions for several physically motivated models for BH growth at high redshift and compared this to the expected LOFAR sensitivity to these sources. The number of potentially detectable HII regions does not only depend on the ionisation state of the intergalactic medium and the decoupling of the spin temperature of the neutral hydrogen from the cosmic microwave background (CMB) temperature, but is also strongly sensitive to the rate of growth of BHs at high redshift. If the supermassive BHs at redshift 6 were built up via continuous Eddington-limited accretion from low mass seed BHs at high redshift, then LOFAR is not expected to detect isolated QSO HII regions at redshifts much larger than 6, and only if the IGM is still significantly neutral. If the high-redshift growth of BHs starts with massive seed BHs and is driven by short-lived accretion events following the merging of BH hosting galaxies then the detection of HII regions surrounding supermassive BHs may extend to redshifts as large as 8 – 9 but is still very sensitive to the redshift to which the IGM remains significantly neutral. The most optimistic predictions are for a model where the supermassive BHs at  $z > 6$  have grown slowly. HII regions around supermassive BHs may then be detected to significantly larger redshifts.

**Key words:** quasars: general - cosmology: theory - intergalactic medium - HII regions

## 1 INTRODUCTION

Reionisation - the change of state of the intergalactic medium (IGM) from a neutral state at recombination to the present day ionised state - is an epoch which is currently under intense study. Analyses of the spectra of high redshift QSOs indicate a smooth increase in the optical depth of the IGM with redshift which accelerates at  $z > 6.1$  (Fan et al. 2002, Songaila 2004, Fan et al. 2006). Quasars at  $z > 6.1$  show almost complete absorption of the flux blue-ward of the Lyman- $\alpha$  resonance [the Gunn-Peterson (1965) effect]. Inferring the ionisation state of the IGM at these high redshifts from QSO absorption spectra is difficult and ambiguous (e.g. Oh & Furlanetto 2005, Bolton & Haehnelt 2006). If the small amounts of flux transmitted just blue-ward of the Lyman- $\alpha$  centre are attributed to the presence of a locally ionised region embedded within a significantly neutral medium, then lower limits on the neutral fraction of

$x_{\text{HII}}$  may be inferred (Wyithe & Loeb 2004a; Mesinger & Haiman 2004). Malhotra & Rhoads (2005), however, argue that the number density of Lyman- $\alpha$  emitters can be used to place a lower limit on the ionised fraction of gas at  $z \sim 6$  at 20 – 50 per cent. Fan et al. (2006) also come to the conclusion that the IGM probed by the highest redshift QSOs is predominantly ionised.

The optical depth to Thomson scattering inferred from the recent WMAP measurements offers an independent constraint on the integrated reionisation history. Interpreted as a sudden reionisation at a redshift  $z_{\text{reion}}$  the year three WMAP results give  $z_{\text{reion}} = 10_{-2.3}^{+2.7}$  (Spergel et al. 2006).

The emerging picture is consistent with the reionisation of cosmic hydrogen being complete by  $z \sim 6 - 13$  and therefore significant contribution to reionisation by sources beyond current detection limits. Experiments to detect the redshifted 21cm signature of high redshift neutral hydrogen will potentially provide copious amounts of information on the epoch of reionisation. The European design for a low frequency interferometer, LOFAR, may be in operation as early as 2007 and other low-frequency experiments (see §5)

\* krhook@ast.cam.ac.uk

† haehnelt@ast.cam.ac.uk

are in various stages of planning and development. However, mapping the high redshift neutral gas distribution in 21cm will be extremely challenging.

The redshifted 21cm signal due to ionised regions produced by bright, high redshift QSOs surrounded by an otherwise still neutral intergalactic medium may be our best bet for an detection of individual objects due to their 21cm signature (see Tozzi et al. 2000 for a detailed discussion). Kohler et al. (2005) used numerical simulations to show that ionised regions around high redshift QSOs are indeed likely to be the most prominent features in the high redshift neutral gas distribution. Wyithe, Barnes & Loeb (2005) use a semi-analytic model for the high redshift QSO HII region distribution and predict detectable HII regions at  $z \sim 6-8$ . However, the growth history of high redshift supermassive BHs is very uncertain. In this paper we will investigate a range of models for high redshift BH growth which reproduce the bright end of the luminosity function of redshift 6 QSOs and sample the range of plausible growth histories at higher redshift.

We begin by reviewing the physics of detecting a 21cm signal due to neutral hydrogen (§2). In section 3 we describe our models for the evolution of the QSO luminosity function (QLF). We discuss the expected size of HII regions due to QSOs in §4. Finally, in §5, we compare our computed size distributions to the expected sensitivity of LOFAR<sup>1</sup> to extended sources and discuss observational prospects.

Throughout this paper we adopt a cosmological matter density  $\Omega_m = 0.27$ , baryonic matter density  $\Omega_b = 0.044$ , cosmological constant  $\Omega_\Lambda = 0.73$ , present day Hubble constant  $H_o \equiv 100h \text{ km s}^{-1} \text{ Mpc}^{-1} = 71 \text{ km s}^{-1} \text{ Mpc}^{-1}$ , a mass variance on scales of  $8h^{-1} \text{ Mpc}$   $\sigma_8 = 0.84$  and a scale invariant primordial power spectrum (slope  $n = 1$ ).

## 2 PHYSICS OF 21CM EMISSION/ABSORPTION

A ground state neutral hydrogen atom can emit or absorb at a wavelength of 21cm corresponding to the energy of the transition between the singlet and triplet hyperfine levels. At the low frequencies of this transition, the specific intensity of the emission is proportional to the brightness temperature of the source  $T_b$  as described by the the Raleigh-Jeans law,

$$I(\nu) = \frac{2\nu^2}{c^2} k_B T_b. \quad (1)$$

The brightness temperature of a typical patch of sky at redshift  $z$  depends on the optical depth of the gas to 21cm radiation, the temperature of the cosmic microwave background  $T_{\text{CMB}}$  and the spin temperature of the gas,

$$T_b = T_{\text{CMB}} e^{-\tau} + (1 - e^{-\tau}) T_s, \quad (2)$$

where  $\tau$  depends on the density and ionisation state of the gas. This results in a differential brightness temperature,

$$\begin{aligned} \delta T_b &= \frac{(T_b - T_{\text{CMB}})}{T_{\text{CMB}}(1+z)} \\ &\approx 27 \text{ mK } x_{\text{HI}} \left(1 - \frac{T_{\text{CMB}}}{T_s}\right) \left(\frac{\Omega_b h^2}{0.02}\right) \\ &\quad \left[\left(\frac{1+z}{10}\right) \left(\frac{0.27}{\Omega_m}\right)\right]^{1/2}. \end{aligned} \quad (3)$$

Significantly neutral hydrogen gas for which  $T_s$  differs from  $T_{\text{CMB}}$  will emit or absorb at 21cm in contrast to the CMB. The value of  $T_s$  is determined by the kinetic temperature of the IGM,  $T_{\text{IGM}}$ , and the strength with which  $T_s$  and  $T_{\text{IGM}}$  are coupled via collisional ionisation and/or Lyman- $\alpha$  pumping.  $T_{\text{IGM}}$  is expected to decouple from  $T_{\text{CMB}}$  as early as  $z \sim 150-200$  as the timescale for Compton scattering off residual free electrons becomes longer than the expansion timescale (e.g. Scott & Rees 1990). In the absence of a heat source, the IGM cools adiabatically below  $T_{\text{CMB}}$  and therefore the very first (Population-III) sources are expected to be born in a cold IGM.

The redshift range over which HII regions will appear in absorption is uncertain; if  $T_s$  couples to  $T_{\text{IGM}}$  prior to significant long range X-ray heating there may be a significant absorption epoch. Furlanetto (2006) argues that if the (thermal) radiation from Pop-II stars dominate reionisation then this will be the case, but if Pop-III stars were dominant in reionising the universe then the IGM could be heated above  $T_{\text{CMB}}$  before there are sufficient Lyman- $\alpha$  photons to couple  $T_s$  to  $T_{\text{IGM}}$  (see also Chen & Miralda-Escudé 2003 and Kuhlen, Madau & Montgomery 2006). For simplicity we assume here that the temperature of the IGM lies well above the temperature of the CMB. Regions of ionised gas then appear as holes in the 21cm emission due to the IGM (see also Kohler et al. (2005) for a more detailed discussion).

With the rise of the galaxy and QSO populations the ionised fraction of gas increases and the 21cm signal emission due to the IGM becomes weaker. The signal will disappear by  $z < 6$  when we know the neutral hydrogen is predominantly ionised. There will be a finite period of time when the IGM is heated above the temperature of the CMB but most of the gas is still neutral. This is the (uncertain) redshift range over which instruments like LOFAR can probe. In addition, the performance of LOFAR will depend on our ability to model and remove foreground contamination due to the ionosphere, our own galaxy, and both extended and point-like extragalactic sources.

## 3 MODELS FOR THE LUMINOSITY FUNCTION OF HIGH REDSHIFT QSOS

### 3.1 The growth of supermassive black holes at high redshift

We are interested here in the HII regions around supermassive BHs at high redshift. Accretion onto a BH is an efficient mechanism for producing ionising photons and therefore a supermassive BH that has been built up by gas accretion should generate a very large ionised bubble. If the ionising flux generated by the supermassive BHs at high redshift exceeds that produced by other sources in the same region then the sites of supermassive BHs will show up prominently

<sup>1</sup> <http://www.lofar.org/>

in 21cm maps as large ionised regions in an otherwise still neutral IGM. In order to estimate the space density and size distribution of these HII regions we require a model for the growth of the supermassive black holes and the production of ionising photons. Our best anchor point for such modelling is the observed luminosity function of  $z = 6$  QSOs. We therefore consider here models which reproduce this luminosity function but differ in the timescale over which the black holes powering the  $z = 6$  QSOs grow.

### 3.2 Passive evolution model

The e-folding time for BH growth at the Eddington limit is  $\sim 0.44(\epsilon_{\text{acc}}/(1 - \epsilon_{\text{acc}}))$  Gyr, where  $\epsilon_{\text{acc}}$  is the fraction of the mass energy released as radiation. Estimates for the mass of seed BHs produced by Population-III remnants are  $\sim 10 - 10^3 M_{\odot}$ . Such seed masses would require  $\sim 15 - 20$  e-foldings to grow to  $3 \times 10^9 M_{\odot}$ , the estimated mass of the black holes powering the observed  $z = 6$  QSOs. The growth of a  $3 \times 10^9 M_{\odot}$  BH by a redshift  $\sim 6$  from a Population-III remnant therefore requires more or less continuous accretion if the accretion rate is limited to the Eddington accretion rate. It is a matter of intense debate whether accretion above the Eddington rate contributes significantly to the growth of supermassive black holes (see Begelman, Volonteri & Rees 2006 for a recent discussion).

We first construct a simple passive evolution model for the growth of supermassive black holes and the evolution of the QSO luminosity function at  $z > 6$  in which a fixed comoving density of black holes accrete at their Eddington limit with a fixed duty cycle  $f_{\text{duty}}$ .

The bolometric luminosity of a QSO powered by a BH of mass  $M_{\text{bh}}$  radiating at the Eddington limit is given by

$$\begin{aligned} L_{\text{bol}} &= \frac{4\pi G c m_{\text{p}} M_{\text{bh}}}{\sigma_e}, \\ &= 3.28 \times 10^4 L_{\odot} \frac{M_{\text{bh}}}{M_{\odot}} \equiv \mathcal{L} L_{\odot} \frac{M_{\text{bh}}}{M_{\odot}}, \end{aligned} \quad (4)$$

where  $\sigma_e$  is the Thompson scattering cross section. The B-band luminosity is assumed to be a fraction  $f_B = 1/10$  of  $L_{\text{bol}}$ . Assuming that a fraction  $\epsilon_{\text{acc}} = 0.1$  of the mass energy of the accreted mass is released as radiation, the ensemble average luminosity evolution with respect to the redshift 6 population is then given by,

$$L(z) = L(z=6) e^{-(t_z=6-t_z) f_{\text{duty}}/\kappa}, \quad (5)$$

$$\begin{aligned} \kappa &= \frac{c \sigma_e}{4\pi G m_{\text{p}}} \frac{\epsilon_{\text{acc}}}{1 - \epsilon_{\text{acc}}}, \\ &\simeq 5 \times 10^8 \text{ yrs} \frac{\epsilon_{\text{acc}}}{1 - \epsilon_{\text{acc}}}, \end{aligned} \quad (6)$$

where  $t_z \equiv t(z)$  is the cosmic time at redshift  $z$ .

We adopt the QLF of §3.3 as our template QLF at  $z = 6$ . In this model all luminosities grow exponentially and the shape of the luminosity function is independent of redshift. We consider two values of the total duty cycle  $f_{\text{duty}} = [0.1, 1.0]$ . To account for a possible contribution to the growth in an optically obscured accretion mode we split the duty cycle of accreting black holes into phases of luminous growth ( $f_{\text{lum}}$ ) and growth in an obscured phase ( $f_{\text{obs}}$ ). We assume the QSO spends equal amounts of time in each phase so that  $f_{\text{lum}} = f_{\text{obs}} = [0.05, 0.5]$ . The observed

lifetime of a QSO in this model is redshift dependent, and depends on the duty fraction of the luminous population,

$$\begin{aligned} t_q &= f_{\text{lum}} t_H(z) \\ &\simeq 3.5 \times 10^8 \text{ yrs} \left( \frac{f_{\text{lum}}}{0.1} \right) \left( \frac{1+z}{7} \right)^{-3/2}. \end{aligned} \quad (7)$$

for  $z \gg 1$ .

Here  $t_H(z) = \frac{2}{3H(z)}$  is the Hubble time at a redshift  $z$  and  $H(z) = H_0[(1+z)^3 \Omega_m + \Omega_{\Lambda}]^{1/2}$  is the Hubble parameter.

### 3.3 A merger driven model

#### 3.3.1 Galaxy mergers as triggers for QSO activity

The activity powering optically bright QSOs is thought to be triggered by galaxy mergers, which drive cold gas onto a central black hole. Various models for the growth of black holes in hierarchically merging galaxies have been built (e.g. Kauffmann & Haehnelt 2000, Volonteri et al. 2003) and have been successful in reproducing the observed QSO luminosity function at  $z < 5$ . These models generally assign a QSO light curve to each merging event, guided by observationally and/or physically motivated estimates for the central black hole mass and associated accretion rate (see Hopkins et al. 2005 for light curves motivated by numerical simulations of a galaxy merger). Below we construct a simple version of such a model for the QLF which uses the (extended) Press-Schechter formalism for dark matter halos to estimate the rate of galaxy mergers (see Erickcek et al. (2006) for a recent critical assessment of the accuracy of the extended Press-Schechter formalism). The model is similar to those described by Haehnelt, Natarajan & Rees (1998) and Wyithe & Loeb (2003).

#### 3.3.2 Estimating merger rates of black holes

Our model makes a number of simplifying assumptions. We assume that the merger rate of black holes is equal to the merger rate of the dark matter halos of the galaxies hosting the black holes as estimated using the (extended) Press-Schechter formalism. We assume a relation of the mass of the BH,  $M_{\text{bh}}$ , and the mass of the dark matter halo forming in a merger  $M$  as motivated by the observed correlation between  $M_{\text{bh}}$  and the velocity dispersion of the host galaxies stellar bulge /dark matter halo,

$$M_{\text{bh}} \propto \sigma^{\alpha}, \quad (8)$$

in nearby galaxies (Gebhardt et al. 2000, Ferrarese & Merritt 2000, Ferrarese 2002). This relation appears to hold independently of redshift for QSOs out to  $z \sim 3$  (Shields et al. 2003, 2006). Empirical estimates of  $\alpha$  typically fall in the range 4 – 5. We have chosen  $\alpha = 5$  which is consistent with a simple self-regulated growth scenario in which the black hole grows until it radiates enough energy to unbind the gas that is feeding it (e.g. Silk & Rees 1998, Haehnelt Natarajan & Rees 1998, Wyithe & Loeb 2003). We further assume that the velocity dispersion of the stellar bulge is proportional to the circular velocity of the dark matter halo at the virial radius,  $\sigma = v_{\text{vir}}/\sqrt{2}$ , with (Barkana & Loeb 2001),

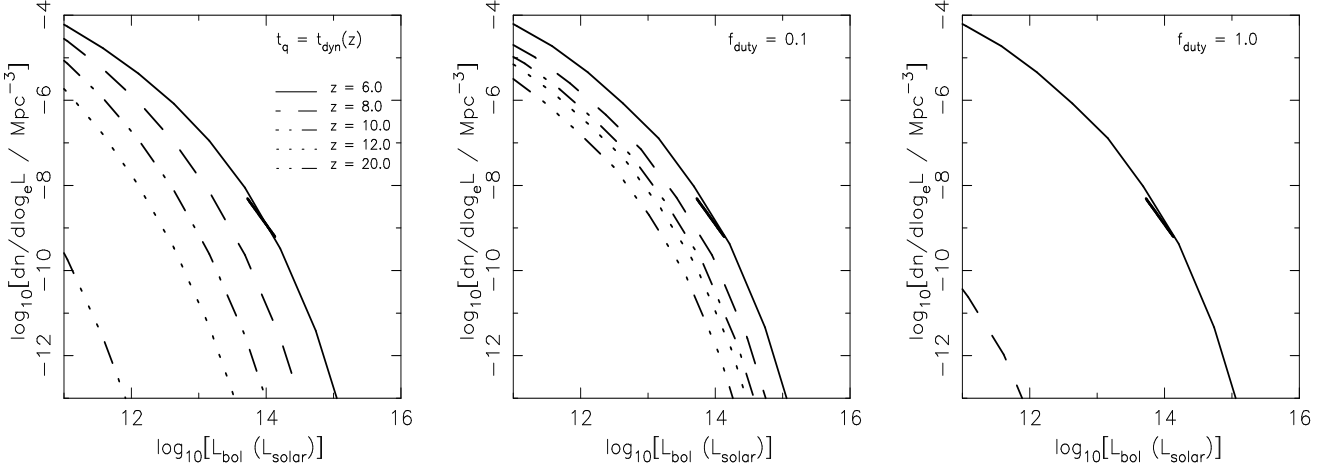


**Figure 1.** The thin curves show the QLF as a function of bolometric QSO luminosity at  $z = 6, 8, 10, 12, 20$  for the merger rate model with  $\epsilon_o = 10^{-4.8}$  (*left panel*), and the passive evolution models with obscured duty fractions equal to the duty fraction of the luminous population and total duty fraction  $f_{\text{duty}} = 0.1$  (*middle panel*) and  $f_{\text{duty}} = 1.0$  (*right panel*). The thick line shows the Fan et al. (2004) fit to the observed  $z \sim 6$  luminosity function at a rest frame wavelength of  $1450\text{\AA}$ , where we have assumed that 10 per cent of the energy is radiated in the B-band and converted to a B-band magnitude using  $M_B = M_{1450} - 0.48 + 5 \log_{10} \left( \frac{h}{0.65} \right)$ . Note that the dashed line in the bottom left corner of panel 3 is the  $z = 8$  QLF.

$$v_{\text{vir}} = 420 \left( \frac{M}{10^{12} h^{-1} M_{\odot}} \right)^{1/3} \left[ \frac{\Omega_m}{\Omega_m^z} \frac{\Delta_c}{18\pi^2} \right]^{1/6} \times \left( \frac{1+z}{7} \right)^{1/2} \text{ kms}^{-1}, \quad (9)$$

where  $\Omega_m^z = \frac{\Omega_m (1+z)^3}{\Omega_m (1+z)^3 + \Omega_{\Lambda} + \Omega_k (1+z)^2}$ ,  $d \equiv \Omega_m^z - 1$  and  $\Delta_c = 18\pi^2 + 82d - 39d^2$  is the overdensity of a virialised halo at redshift  $z$ . Equations (8) and (9) lead to a dependence of black hole mass on host halo mass  $M$  and redshift of the form,

$$M_{\text{bh}} = \epsilon(M, z) M = \epsilon_o h^{\alpha/3} \left[ \frac{\Omega_m \Delta_c}{\Omega_m^z 18\pi^2} \right]^{\alpha/6} \times (1+z)^{\alpha/2} \left( \frac{M}{10^{12} M_{\odot}} \right)^{\alpha/3-1} M. \quad (10)$$

Note that  $\epsilon_o$  sets the ratio of  $M_{\text{bh}}/M$  for a given redshift.

Assuming that all dark matter halos host a central BH with mass given by equation (10), the merging rate of halos of mass  $(M - \Delta M)$  and  $\Delta M$  is equal to the merger rate of halos hosting BHs of mass  $(M_{\text{bh}} - \Delta M_{\text{bh}})$  with those hosting BHs of mass  $\Delta M_{\text{bh}}$  for  $\Delta M_{\text{bh}} = \epsilon(\Delta M, z(t)) \Delta M$  and  $M_{\text{bh}} = \epsilon(M, z(t)) M$ .  $N_{\text{halo}}(M, \Delta M, t)$  is given by the product of the probability per unit time that a halo mass  $\Delta M$  will merge with another halo to form a halo with mass  $M$  and the space density of halos with the appropriate mass difference,

$$N_{\text{halo}}(M, \Delta M, t) = \frac{d^2 P}{d\Delta M dt} \Big|_{M-\Delta M} \frac{dn}{d(M-\Delta M)} \quad (11) = N_{\text{bh}}(M_{\text{bh}}, \Delta M_{\text{bh}}, t).$$

The mass density is derived from the Press-Schechter (1974) halo mass function with the modification described by Sheth & Tormen (1999) and the halo merger probability is taken from the extended Press-Schechter formalism (Lacey & Cole 1993).

### 3.3.3 From merger rate to luminosity function

We assume that following a merger, each black hole accretes and radiates at its Eddington limit for a period equal to the dynamical time of gas in a disk of radius 0.035 times the virial radius as in Wyithe & Loeb 2003,

$$t_q = t_{\text{dyn}}(z) = 10^7 \text{ yrs} \left[ \frac{\Omega_m}{\Omega_m^z} \frac{\Delta_c}{18\pi^2} \right]^{-1/2} \left( \frac{1+z}{3} \right)^{-3/2}, \quad (12)$$

The light curve is assumed to be a simple top-hat function  $L(M_{\text{bh}}, t)/L_{\odot} = \mathcal{L} M_{\text{bh}}/M_{\odot} \Theta[t_q - (t - t_z)]$  (with  $\Theta$  the usual Heaviside step function).

The QLF can then be estimated by integrating over the merger rate of all BH pairs as follows,

$$\Phi(L, z) = \int_0^{\infty} dM_{\text{bh}} \int_{0.25\epsilon M}^{0.5\epsilon M} d\Delta M_{\text{bh}} \int_z^{\infty} dz' \frac{dt'}{dz'} \quad (13) \times N_{\text{bh}}(M_{\text{bh}}, \Delta M_{\text{bh}}, t') \delta[L - L(M_{\text{bh}}, t)].$$

If we perform the integral over  $M_{\text{bh}}$  using the  $\delta$  function, use equation (10) to make the change of variable from

BH masses to halo masses and assume that the merger rate changes little over the QSO lifetime [i.e.  $t_q \ll t_H(z)$ ], we get (see Wyithe & Loeb 2003),

$$\Phi(L, z) = \frac{\int_{0.25M}^{0.5M} d\Delta M N(M, \Delta M, t(z)) t_q \frac{3}{\alpha \epsilon}}{\mathcal{L} L_{\odot} M_{\odot}^{-1}}, \quad (14)$$

where  $L/L_{\odot} = \mathcal{L}\epsilon(M, z)M/M_{\odot}$ . Note that the integral over  $\Delta M$  is truncated at the lower end to ensure that we are only counting major mergers and at the upper end to count each potential halo merger pair only once.

In principle,  $\alpha$ ,  $\epsilon_o$  and  $t_q$  may be tuned to fit our model QLF to the observed QLF at  $z \sim 6$ . We have fixed  $\alpha = 5$  and  $t_q = t_{\text{dyn}}(z)$  and varied  $\epsilon_o$  to fit to the observed luminosity function. For  $\epsilon_o = 10^{-4.9}$  we obtain an acceptable fit to the observed luminosity function (see Figure 1). This normalisation is consistent with the corresponding empirical normalisation of equation (8) for galaxies in the local universe ( $\epsilon_o \approx 10^{-4.9}$ , see Ferrarese 2002).

Note that with the assumption  $t_q = t_{\text{dyn}}$  the QSO lifetime at  $z = 6$  is  $\approx 1.3 \times 10^7$  yrs, which is consistent with other estimates of the duration of the optically bright phase of QSOs (Haehnelt, Natarajan & Rees 1998, Haiman & Hui 2001, Martini & Weinberg 2001, Hopkins et al. 2005). Note that the shorter lifetime in the merger driven model compared to the passive evolution model results in smaller HII regions for the assumed values of  $f_{\text{duty}}$ .

### 3.4 Comparison with observations

#### 3.4.1 Quasar luminosity function

Figure 1 shows the evolution of our model QSO luminosity function at  $z > 6$  (the passive evolution model with two values of the duty cycle and the merger driven model). By construction all models agree with the observed space density of bright QSOs at  $z \sim 6$  as determined by Fan et al. (2004). The redshift evolution differs dramatically for the three models. Fan et al. (2001) find that the observed space density of bright QSOs decreases with redshift like  $e^{-1.15z}$  for  $3.6 < z < 6$ . We compare this to the redshift evolution in our model QLFs by summing over the bright end of each QLF. We sum from a minimum luminosity  $L_{\text{bol}} = 5.3 \times 10^{13} L_{\odot}$  which corresponds to a rest frame  $1450\text{\AA}$  absolute magnitude of  $-26.8$  [for a conversion to B-band magnitude  $M_B = M_{1450} - 0.48 + 5 \log_{10} \frac{h}{0.65}$  (Fan et al. 2001)]. The results are displayed in Figure 2. For the merger driven model the density of QSOs declines with a similar slope to the decline in the observed space density at lower redshift. In the passive evolution model the rate of decline depends sensitively on the assumed duty fraction. For the lower value of the assumed duty cycle ( $f_{\text{duty}} = 0.1$ ) the black holes grow relatively little at high redshift and the drop in the space density of bright QSOs is significantly slower than in the merger driven model. For the high value of the duty cycle ( $f_{\text{duty}} = 1$ ) the QSOs are growing rapidly and quickly decline in luminosity at higher redshift. As we will discuss in more detail below the three models span a wide range of possible growth histories of supermassive black holes at high

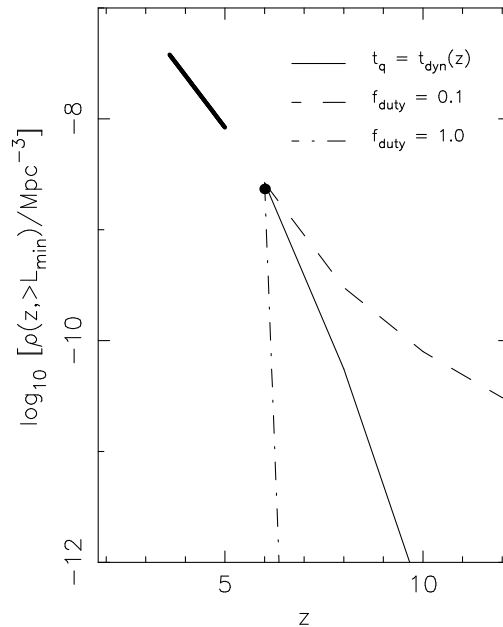


**Figure 2.** Redshift evolution of QSO space density for each of the three models plotted in Figure 1; the merger rate model with lifetime of  $t_q = t_{\text{dyn}}(z)$  from equation (12) (*thin solid line*), the passive evolution model with fixed duty cycle  $f_{\text{duty}} = 0.1$  (*dashed line*) and  $f_{\text{duty}} = 1.0$  (*dot-dashed line*). The *solid thick line* shows the evolution found for SDSS QSOs in the redshift range  $3.6 < z < 5$  (see Fan et al. 2004) and the *dot* is the estimated space density of QSOs at  $z = 6$  (Fan et al. 2004). We have taken  $L_{\text{min}} \approx 5 \times 10^{13} L_{\odot}$  which is the bolometric luminosity corresponding  $M_{1450} = -26.8$  assuming that  $M_B = M_{1450} - 0.48 + 5 \log_{10} \left( \frac{h}{0.65} \right)$  and ten per cent of the bolometric luminosity is radiated in the B-band.

redshift. We should also note that all three models overpredict the space density of bright QSOs at lower redshifts. As discussed in detail by Bromley, Somerville & Fabian (2004) the rapid growth history of supermassive black holes at high redshift is not easily reconciled with the much slower observed growth at low redshift which is normally modelled with rather severe feedback effects due to energy input by stars and/or the black hole. As we are only interested in the growth of supermassive black holes before reionisation we make no attempt to model this here.

#### 3.4.2 Black hole mass densities and accretion rates

The accretion rate of mass onto black holes during the optically bright phase of accretion can be extracted from the optical QLF as follows,

$$\frac{d\rho_{\text{acc, lum}}}{dz} dz = \int_{z+dz}^z dz' \frac{dt}{dz'} \int dL \frac{dn}{dL}(z') L(z') \frac{1 - \epsilon_{\text{acc}}}{\epsilon_{\text{acc}} c^2}. \quad (15)$$

An approximation to the total mass density in BHs can be extracted from the model luminosity function by dividing the luminosity function by the fraction of luminous/active halos at a given time  $f_{\text{lum}}(L, z)$ ,

$$\rho_{\text{bh}}(z) = \frac{1}{\mathcal{L} L_{\odot} M_{\odot}^{-1}} \int dL \frac{dn}{dL} \frac{L}{f_{\text{lum}}(L, z)}. \quad (16)$$

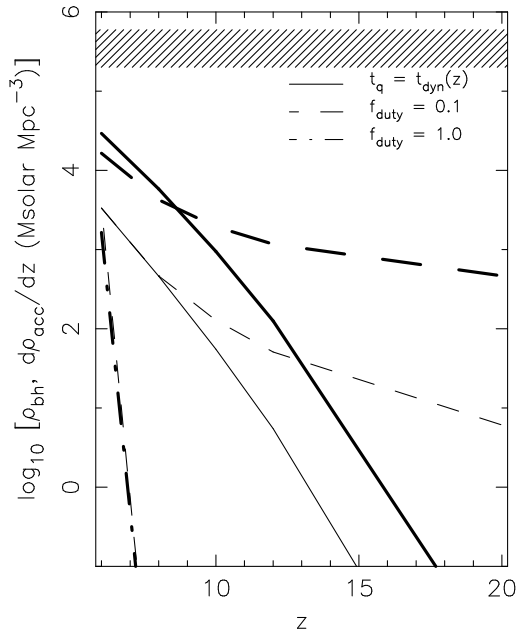


**Figure 3.** Redshift evolution of the mass density in black holes (*bold lines*) and observed accretion rate of matter onto black holes (*thin lines*) as described in §3.4 for the three models described in §3. The *hatched* regions shows the range of estimates for the mass density in BHs at  $z = 0$  (Yu & Tremaine 2002).

For the passive evolution model  $f_{\text{lum}}$  is assumed to be constant. Note, however, that this will somewhat overestimate the BH mass density. For the merger rate model  $f_{\text{lum}}$  is estimated to be the ratio of the QSO lifetime to the average survival time of a dark matter halo as a function of halo mass and redshift [ $t_s(M, z)$ ] calculated from the probability distribution in equation (2.21) of Lacey & Cole (1993). At low redshift  $t_s$  is approximately the Hubble time, but it decreases to 30 per cent of the Hubble time by  $z \sim 12$  for the relevant halo masses. Figure 3 shows the evolution of the black hole mass density and the rate of mass accretion during optically bright phases for our three models. As expected the evolution differs strongly between the three models. We also show the observed black hole mass density at  $z = 0$  which is about 30 – 300 times larger than our estimates at  $z = 6$ . The difference in the integrated observed accretion rate and the mass density in BHs is due to the assumed periods of obscured QSO accretion. By construction the integrated luminous accretion rate will fall short of the mass density in black holes in the passive evolution models by a factor  $f_{\text{duty}}/f_{\text{lum}} = 2$  at  $z = 6$ . In our merger driven model this difference is much larger. Approximately ten per cent of the inferred BH mass density is accumulated due to luminous accretion. In this model approximately 90 per cent of the growth would have to occur in an obscured phase. Such a growth scenario is consistent with the findings of Hopkins et al. (2005) based on hydrodynamical simulations of QSO activity fuelled by merging disk galaxies.

#### 4 HII REGIONS AROUND HIGH REDSHIFT SUPERMASSIVE BLACK HOLES

Assuming that the QSO is embedded in a homogeneous gas distribution with neutral hydrogen number density  $\bar{n}_H = x_{\text{HI}}\bar{n}_{H,o}(1+z)^3$ , the increase of the physical volume of ionised hydrogen  $V_{\text{HII}}$  generated by an ionising flux  $\dot{N}_{\text{ion}}(t)$  is given by (e.g. Madau, Haardt & Rees 1999, hereafter MHR99),

$$\frac{dV_{\text{HII}}}{dt} - 3H(t)V_{\text{HII}} = \frac{\dot{N}_{\text{ion}}(t)}{\bar{n}_H(t)} - \frac{V_{\text{HII}}}{\bar{t}_{\text{rec}}(t)}, \quad (17)$$

We assume the cosmic abundance of hydrogen with a neutral fraction  $x_{\text{HI}}$  and that the temperature of the ionised IGM ( $T_{\text{IGM}}$ ) is  $10^4$  K. The average hydrogen recombination timescale  $\bar{t}_{\text{rec}}$  for such a gas is (see Abel et al. 1997),

$$\bar{t}_{\text{rec}} = 3 \times 10^8 \text{ yrs} \left( \frac{T_{\text{IGM}}}{10^4 \text{ K}} \right)^{0.7} \left[ \frac{1+z}{7} \right]^{-3} \left( \frac{C_{\text{eff}}}{3} \right)^{-1}, \quad (18)$$

where we have assumed an effective clumping factor  $C_{\text{eff}} = 3$ . The effective clumping factor relevant for recombinations is expected to be low since the densest self-shielded regions of neutral gas have a small covering factor and should not impede the progression of the ionisation front (see Miralda-Escudé, Haehnelt & Rees 2000 for a detailed discussion).

Equation (17) is integrated numerically to solve for the physical radius of the HII regions for QSOs in each of our QLF models,

$$R_{\text{HII}} = \left( \frac{3}{4\pi} \int_{t(z)-t_q}^{t(z)} \frac{dV_{\text{HII}}}{dt} \right)^{1/3}. \quad (19)$$

Equation (17) is approximately equivalent to assuming that the volume of the ionised region is equal to the ratio of the number of emitted ionising photons and the density of neutral hydrogen,

$$V_{\text{HII}} \approx \frac{\dot{N}_{\text{ion}} > t_q}{\bar{n}_H}. \quad (20)$$

For a QSO with constant luminosity, this approximation breaks down as  $t_q \rightarrow \bar{t}_{\text{rec}}$  and the HII region reaches its Strömgen radius. However for a QSO with luminosity growing exponentially with the mass of the central BH, most of the HII region growth occurs between  $t(z) - \kappa$  and  $t(z)$ . Since  $\kappa \sim \bar{t}_{\text{rec}}$ , the result holds for the QSOs with  $t_q > \bar{t}_{\text{rec}}$  in our models. Note that since little ionising flux is produced early in the lifetime of a QSO powered by a BH continually accreting at the Eddington limit, the size of the HII regions at  $z = 6$  are approximately equal for each of the passive evolution models even though the lifetimes differ by a factor of 10.

For each of our models the radial extent of the ionised region generated by a QSO depends inversely on the surrounding neutral hydrogen fraction  $x_{\text{HI}}$  and increases with the QSO luminosity as  $R_{\text{HII}} \propto L_{\text{bol}}^{1/3} x_{\text{HI}}^{-1/3}$ .

We calculate  $\dot{N}_{\text{ion}}$  at all redshifts by assuming the optical/UV spectral energy distribution [ $L(\nu)$ ] as given by MHR99 with a high energy cut-off of 200 keV. The spec-

tral energy distribution is normalised by assuming  $\nu_B L_B = f_B L_{\text{bol}}$  (with  $f_B = 0.1$  as in §3). This gives an ionising flux,

$$\dot{N}_{\text{ion}} = \int_{\nu_{\text{ion}}}^{\infty} \frac{L(\nu)}{h\nu} d\nu \approx 1.5 \times 10^{57} \text{ s}^{-1} \left( \frac{L_{\text{bol}}}{10^{14} L_{\odot}} \right), \quad (21)$$

where  $\nu_{\text{ion}}$  is the minimum photoionising frequency. The corresponding radius of the HII region, for a QSO with constant luminosity is,

$$R_{\text{HII}} = 3.6 \text{ Mpc} (x_{\text{HI}})^{-1/3} \left( \frac{L_{\text{bol}}}{10^{14} L_{\odot}} \right)^{1/3} \times \left[ \frac{t_q}{1 \times 10^7 \text{ yrs}} \right]^{1/3} \left( \frac{1+z}{7} \right)^{-1}. \quad (22)$$

## 5 PROSPECTS FOR DETECTING HIGH REDSHIFT HII REGIONS

### 5.1 Future high-redshift 21cm experiments

The next generation of radio telescopes are aiming to explore the low-frequency universe, with detection of an epoch of reionisation signal a major scientific goal. Various low-frequency interferometers are being designed, tested and built with some already taking data. The largest radio telescope on the horizon is the Square Kilometre Array (SKA<sup>2</sup>). The SKA is still in the design phase and not expected to be in operation for more than a decade. However there are several smaller-scale telescopes including LOFAR (to be built in the Netherlands), the Mileura Wide-Field Array (MWA<sup>3</sup>, sited in Western Australia) and the Primeval Structure Formation telescope (PAST<sup>4</sup>, currently being built in China) that are expected to be in operation on much shorter time-scales. These arrays are typically composed of  $\sim \text{few} \times 10^3$  dipoles (with approximately 10 per cent of the collecting area and therefore sensitivity of the tentative SKA design) spread over a region with maximum baseline  $\sim 1$  km and designed to operate at subsets of the frequency range 50–300 MHz. Below we focus on the possibility of detecting HII regions with LOFAR, but our results are easily transferred to alternate designs for a low-frequency interferometer.

### 5.2 LOFAR sensitivity to HII regions

We assume that the ionised region has a brightness temperature contrast of  $\delta T_{\text{HII}} = 27 \text{ mK} [(1+z)/10]^{1/2}$ , corresponding to the limit where the hydrogen in the surrounding IGM is completely neutral, and the spin temperature ( $T_s$ ) of the surrounding neutral gas is efficiently coupled to the kinetic temperature of a warm IGM.

The compact LOFAR core, rather than the full array, will offer the highest sensitivity to extended structures. In the following we have adopted array parameters corresponding to the published design study of LOFAR<sup>5</sup>. Assuming a

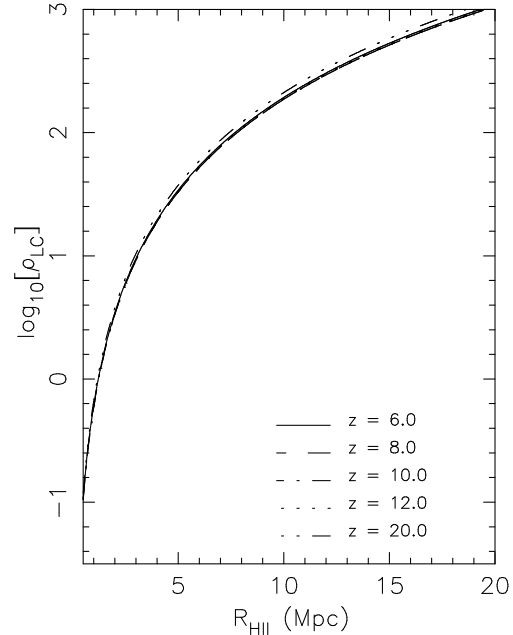


**Figure 4.** Signal to noise ratio as a function of physical radius for spherical HII regions at  $z = 6, 8, 10, 12, 20$ . The calculation assumes constant sky noise at 250 K, 100 hours integration time, a spectral resolution of 0.1 MHz, a top hat beam with the same diameter as the source, and an observed bandwidth which encompasses the source.

spectral resolution  $\Delta\nu_{\text{ch}}$  and integration time  $\Delta\tau$ , an array of  $N_{\text{stn}}$  dual polarisation antennae, each with collecting area  $A_{\text{eff}}$  and system temperature  $T_{\text{sys}}$ , will have a brightness temperature sensitivity

$$\begin{aligned} \Delta T_b(B_{\text{max}}) &= \frac{\sigma_p B_{\text{max}}^2}{2k_B \Gamma}, \\ &\approx 128 \text{ mK} \left( \frac{T_{\text{sys}}}{250 \text{ K}} \right) \left( \frac{\Delta\nu_{\text{ch}}}{0.1 \text{ MHz}} \right)^{-1/2} \left( \frac{\Delta\tau}{100 \text{ hr}} \right)^{-1/2} \\ &\quad \times \left[ \frac{B_{\text{max}}}{2 \text{ km}} \right]^2 \left( \frac{N_{\text{stn}}}{3200} \right)^{-1} \left[ \frac{A_{\text{eff}}}{18 \text{ m}^2} \right]^{-1} \Gamma^{-1}, \end{aligned} \quad (23)$$

where  $B_{\text{max}}$  is the maximum distance between antennae in the core of the array,  $\Gamma = \Omega_{\text{beam}}/(\lambda/B_{\text{max}})^2$  and  $\Omega_{\text{beam}}$  is the solid angle of the synthesised beam.  $k_B$  denotes the Boltzmann constant. The sensitivity to point sources  $\sigma_p$  is given by,

$$\begin{aligned} \sigma_p &\approx 8.8 \times 10^{-5} \text{ Jy} \left( \frac{T_{\text{sys}}}{250 \text{ K}} \right) \left( \frac{\Delta\nu_{\text{ch}}}{0.1 \text{ MHz}} \right)^{-1/2} \\ &\quad \times \left( \frac{\Delta\tau}{100 \text{ hr}} \right)^{-1/2} \left[ \frac{A_{\text{eff}}}{18 \text{ m}^2} \right]^{-1} \left( \frac{N_{\text{stn}}}{3200} \right)^{-1}. \end{aligned}$$

LOFAR is expected to have a bandwidth of 4 MHz with a spectral resolution of 4 kHz which will likely be binned into  $\sim 0.1$  MHz channels. The spatial resolution of the LOFAR core will be inversely proportional to the maximum distance between the antennae ( $\theta_{\text{res}} \approx \lambda/B_{\text{max}} \sim 2.5 \text{ arcmins} \frac{(1+z)}{7}$ ). In comparison, the angular size ( $\theta_{\text{HII}}$ ) and frequency depth ( $\Delta\nu_{\text{HII}}$ ) of an HII region with radius  $R_{\text{HII}}$  are given by

<sup>2</sup> <http://skatelescope.org/>

<sup>3</sup> <http://haystack.mit.edu/arrays/MWA>

<sup>4</sup> <http://web.phys.cmu.edu/past/>

<sup>5</sup> <http://www.lofar.org>

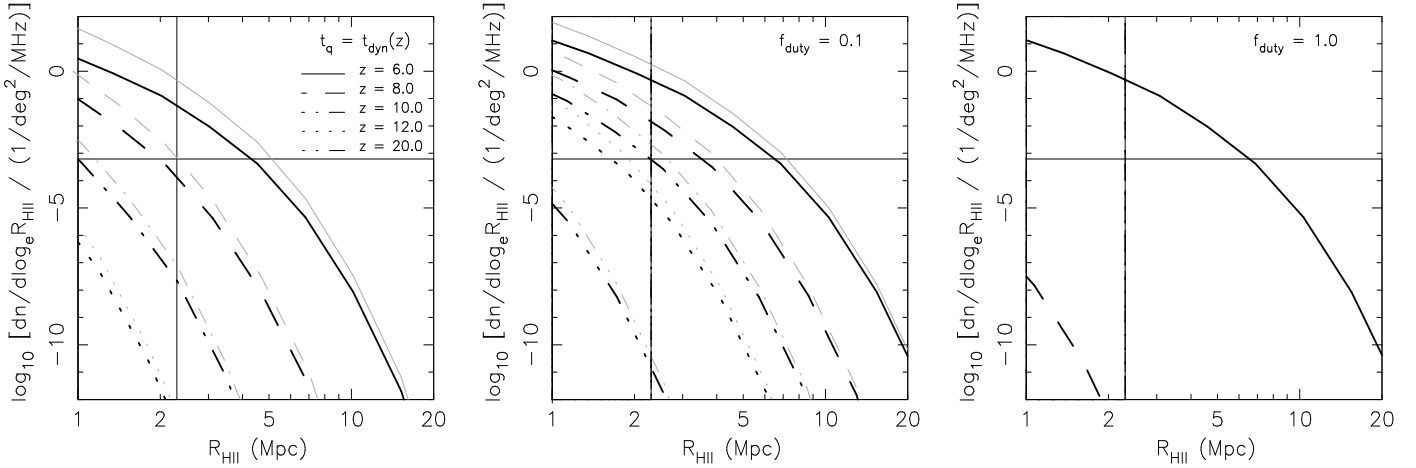


**Figure 5.** The *black* lines show the size distribution of HII regions (physical radius) around active QSOs for  $z = 6, 8, 10, 12, 20$  for the QLFs in Figure 1. The *grey* lines show the size distribution if fossil HII regions are included. The horizontal line corresponds to a source density of one per 400 deg<sup>2</sup> per 4 MHz of observed bandwidth. The vertical line corresponds to the smallest HII region at  $z = 6$  detectable in 100 hours of integration time, as calculated in §5.2, however we find that the minimum detectable physical size changes very little with redshift. Note that the surrounding IGM has been assumed to be neutral.

$$\begin{aligned} \theta_{\text{HII}} &= 2 \frac{R_{\text{HII}}}{D_c(z)} (1+z), \\ &\simeq 14 \text{ arcmins} \left( \frac{R_{\text{HII}}}{5 \text{ Mpc}} \right) \left( \frac{1+z}{7} \right) \left[ \frac{D_c(z)}{D_c(z=6)} \right]^{-1}, \end{aligned} \quad (24)$$

$$\begin{aligned} \Delta\nu_{\text{HII}} &= 2 \frac{H(z)}{c} \frac{R_{\text{HII}}}{1+z} \nu_o, \\ &\simeq 4.6 \text{ MHz} \left( \frac{R_{\text{HII}}}{5 \text{ Mpc}} \right) \left( \frac{1+z}{7} \right)^{-1} \left[ \frac{H(z)}{H(z=6)} \right], \end{aligned} \quad (25)$$

where  $\nu_o \approx 1420$  MHz is the rest-frequency of the signal and  $D_c(z)$  is the comoving distance to a source at redshift  $z$ .

We now calculate the signal to noise ratio (SNR) with which a spherical bubble of a given radius at a certain redshift can be detected with  $N_{\text{stn}} = 3200$  antennae each with  $A_{\text{eff}} = 18 \text{ m}^2$  in a circle of variable diameter  $B_{\text{max}}$ . The brightness temperature sensitivity increases with the compactness of the array. The surface brightness sensitivity will be maximal when the size of the beam is the same as the angular size of the source  $B_{\text{max}} \sim \lambda_{21\text{cm}}/\theta_{\text{HII}}$ ,  $\Gamma = 1$ .

The SNR for a spherical HII region is then given by,

$$\rho_{\text{LC}} \approx \frac{\delta T_{\text{HII}}}{\Delta T_b(B_{\text{max}} = \lambda_{21\text{cm}}/\theta_{\text{HII}})} \left( \frac{\Delta\nu_{\text{HII}}}{\Delta\nu_{\text{ch}}} \right)^{1/2} \mathcal{F}_{\text{HII}}. \quad (26)$$

The factor  $\mathcal{F}_{\text{HII}}$  accounts for the fraction of the beam that is filled with ionised gas. For a spherical top heat beam  $\mathcal{F}_{\text{HII}} = \frac{4/3\pi R_{\text{HII}}^3}{2\pi R_{\text{HII}}^3} = 2/3$ .  $\mathcal{F}_{\text{HII}}$  may be adjusted for different array patterns/synthesised beams and different HII region geometries.

This prescription allows us to estimate the signal to noise ratio for detection of an HII region as a function of its redshift and radius. Figure 4 shows the calculated signal to noise ratio as a function of the physical radius of an HII

region at various redshifts. Note that the increase of SNR with size of the HII region will become shallower once the size exceeds the beam size for the most compact configuration possible. This calculation indicates that the smallest bubble surrounded by a neutral IGM that may be detected at the  $5 - \sigma$  level is  $\sim 2.3$  Mpc at  $z = 6$ . The minimum radius changes very little with source redshift, and turns over at  $z \sim 10$  due to the dependence on the angular diameter distance.

Unfortunately, instrumental noise is not the only type of noise relevant for the detection of HII regions. Residuals from the subtraction of extragalactic and galactic foregrounds and the correction of the distortion of the signal by the ionosphere will all contribute to the noise. We currently have little idea how large the noise due to these residuals will be. The intensity fluctuations in the 21cm emission due to density fluctuations of the IGM will also act as noise (e.g. Kohler et al. 2005, Mellema et al. 2006). For 100 hour integrations with the LOFAR core the fluctuations due to the IGM surrounding the source limit the sensitivity on scales larger than  $\sim 6$  arcminutes (Wyithe, Loeb & Barnes 2005); increasing the exposure time will not significantly decrease the minimum size of detectable HII regions. Furthermore, the edge of an HII region surrounding a QSO is not expected to be sharp (see Zaroubi & Silk 2005) and the intrinsic shape will appear distorted due to light travel time effects (see Wyithe & Loeb 2004b; Yu 2005). The signal to noise ratios estimated here should thus be considered as (probably rather optimistic) upper limits.

### 5.3 The space density of HII regions

In Figure 5 we show our predictions for the space density of HII regions as a function of size at  $z > 6$  in units of deg<sup>-2</sup>MHz<sup>-1</sup> for each of the three models. The vertical and



horizontal lines show the typical size of a LOFAR observing volume ( $\sim 400 \text{ deg}^2$  and 4 MHz of bandwidth) and our estimate for the  $5 - \sigma$  detection threshold for the size. The effective recombination timescale for hydrogen gas at  $10^4 \text{ K}$  is comparable to or somewhat shorter than the Hubble time. As discussed by Wyithe, Loeb & Barnes (2005) HII regions are thus expected to remain as 'fossils' for some time after the QSO turns off. We assume that the HII regions continue to expand with the Hubble flow once the quasar turns off and there are no further recombinations, and count the number of fossil regions with physical radius  $R$  at  $z$  by summing over the size distribution function at redshift intervals corresponding to the quasar lifetime. We assume that the quasars at  $z = 6$  are on average half way through their optically luminous lifetime. There are essentially no fossil HII regions in the case of  $f_{\text{duty}} = 1.0$  since the QSO luminosity grows exponentially on a timescale comparable to the quasar lifetime. Note that for the other two models  $1/f_{\text{fossil}}(R, z)$  is  $\sim 4$  times smaller than  $1/f_{\text{lum}}$  for the smallest HII regions (corresponding to the faintest quasars,  $L_{\text{bol}} \sim 10^{11} L_{\odot}$ ) at  $z = 6$  due to the rapid evolution of the space density of QSOs.  $1/f_{\text{fossil}}(R, z)$  asymptotes to one for large HII regions and high redshifts as expected. We show both the number of HII regions around active QSOs (black lines) and the total number (including fossil bubbles) of HII regions (grey lines). We have assumed that the IGM is still neutral all the way down to  $z = 6$ . We will come back to this point below.

For the merger-driven model we predict  $\sim 14$  detectable sources around active QSOs per LOFAR field at  $z = 6$ . This number increases to  $\sim 340$  if we include fossil HII regions around supermassive black holes which are no longer active. The numbers are similar to those reported by Wyithe, Loeb & Barnes (2005) for their similar model. In our merger driven model at least one detectable HII region per LOFAR field is predicted out to  $z \sim 7$ . Due to the steep slope of the QLF at high luminosities, the numbers would decrease more rapidly with redshift if the effective minimum detectable radius is larger than we have estimated.

For our two passive evolution models the predictions are quite different. The model with the lower duty cycle offers a more optimistic picture than the merger driven model. The longer QSO lifetime results in larger HII regions for the same QSO luminosity. We predict  $\sim 135$  detectable HII regions per LOFAR field at  $z \sim 6$  around active luminous QSOs and detectable HII regions are present up to  $z \sim 10$ . The value of the maximum redshift depends sensitively on the duty cycle and could be – at least in principle – much larger for smaller values of the duty cycle. This would, however, require the formation of very massive black holes at very high redshift which would be difficult in most formation scenarios.

The passive evolution model with the higher value of the duty cycle depicts a much more pessimistic scenario. The predicted numbers at  $z = 6$  are similar to the other models, but the the presence of detectable HII regions does not extend much beyond  $z = 6$ . This is easily explained by the very recent growth of the  $z = 6$  supermassive black holes in this model.

Figure 6 shows the redshift evolution of detectable active and fossil HII regions with  $R_{\text{min}} = 2.3 \text{ Mpc}$ . Clearly the prospects for detecting HII regions depend sensitively on how BHs grow at high redshift.

So far we have assumed that the IGM is still neutral

all the way down to  $z = 6$ . However the neutral fraction at redshift 6 is uncertain and the Universe may already be highly ionised at  $z \sim 6 - 7$  (Malhotra & Rhoads 2005, Fan et al. 2006). A smaller but still significant neutral fraction would result in a larger HII region [see equation (22)], however the signal to noise ratio for the detection of a resolved HII regions scales with the square root of the neutral fraction ( $\rho_{\text{LC}} \propto x_{\text{HI}}^{1/2}$ ); sources in a partially neutral IGM are more difficult to detect.

For consistency we have calculated the volume filling factor of hydrogen ionised by the QSOs in each of our models. We assume that our model extends to QSOs as faint as  $L_{\text{bol}} = 10^{11} L_{\odot}$ , include the contribution due to fossil regions and neglect recombinations. Our filling factor should therefore represent an upper limit on the expected value. We find a filling factor of HII regions generated by the UV emission of active quasars in our models which is less than  $\sim 35$  per cent at  $z \sim 6$  for the model with the low duty fraction and for the merger model and  $\sim 5$  cent for the model with the large duty fraction. For each model the filling factor drops rapidly at higher redshift. Note again that we have integrated down to rather faint quasars and that taking recombinations into account would also lower these values. Our assumption that the HII regions generated by QSOs are isolated may therefore be somewhat questionable at  $z \sim 6$  but should be reasonable at  $z \gtrsim 7$ . Not surprisingly the quasars in our models which are consistent with the rather low observed space density of QSOs at  $z \sim 6$  alone are barely able to fully reionise hydrogen by  $z \sim 6$ .

The quasars should also contribute to the ionisation of hydrogen with their X-ray emission. Due to their long mean free path, X-rays will lead to a more uniform ionisation which includes the low-density IGM far away from the quasars (e.g. Madau et al. 2004, Ricotti & Ostriker 2004). The efficiency with which an X-ray photon ionises hydrogen atoms in the IGM depends on the average number of ionisations induced by secondary electrons, which is a function of the initial photon energy as well as the existing ionised gas fraction (see Shull & van Steenberg 1985). We follow Ricotti & Ostriker and assume that each photon with energy  $\gtrsim 1 \text{ keV}$  results in 10 ionisations in a partially ionised IGM. Assuming again that our model extends to quasars as faint as  $L_{\text{bol}} = 10^{11} L_{\odot}$  the mean ionised fraction at  $z = 6$  due to the X-ray emission of active QSOs in our model is less than 1 percent for all models.

Another possibly relevant effect is the clustering of QSOs. Bright sources are sufficiently rare that clustering should not be important. For fainter sources overlap of clustered HII region could increase the sizes compared to our estimates in particular if fossil HII regions are taken into account.

## 6 CONCLUSIONS

We have investigated the prospects of using the 21cm signature of the regions around supermassive black holes at  $z > 6$  to probe the growth history of these supermassive black holes and the ionisation history of their surrounding IGM.

We have presented three simple, physically motivated models for the high redshift growth history of supermassive

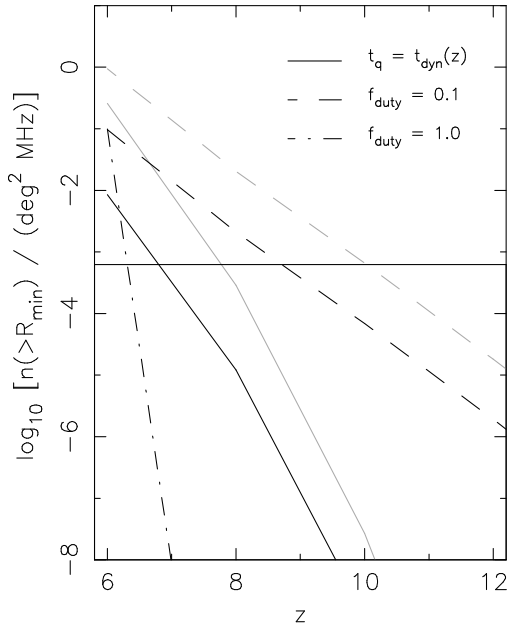


**Figure 6.** Number of HII regions larger than the calculated optimal detection limit of  $R_{\min} = 2.3$  Mpc detectable limit as a function of redshift for the merger driven model (*solid* line) and passive evolution models with  $f_{\text{duty}} = 0.1$  (*dashed* line) and  $f_{\text{duty}} = 1$  (*dot-dashed* line). The *black* lines correspond to HII regions around active QSOs and the *grey* lines include fossil HII regions. The horizontal line corresponds to one source per 400  $\text{deg}^2$  field of view per 4 MHz bandpass. Note that the surrounding IGM has been assumed to be neutral.

black holes in which the growth is either simple Eddington limited accretion or due to short-lived accretion phases triggered by the merger of galaxies. We have used a simple analytical model for the size of HII regions in order to generate predictions for the size distribution of HII regions for each of our model QLFs. Our results show that models which are all consistent with the luminosity function of bright QSOs at  $z = 6$  but differ in the growth history of the supermassive black holes give very different results for the predicted number of detectable HII regions.

Our estimates for the number of detectable HII regions at  $z \sim 6$  are promising, up to several hundred detectable sources per LOFAR field around active QSOs and possibly many more fossil regions. However, the number of detectable HII regions depends sensitively on unknown details of SMBH growth and the ionisation state of the IGM. If the QLF evolves to  $z > 6$  as predicted in our merger-driven model, then isolated HII regions will be prominent features of the high redshift neutral hydrogen distribution providing reionisation was completed late ( $z < 7$ ). However if the SMBH population is growing rapidly due to continuous accretion, or reionisation occurred much earlier than  $z \sim 6$ , then the detection of QSO HII regions may prove elusive.

The most optimistic picture emerges if supermassive black holes grow more slowly over an extended period of time as in our Eddington limited accretion model with a smaller duty cycle ( $f_{\text{duty}} = 0.1$ ). In this case detectable sources may be present to very large redshifts and the prospects for detection are good even if reionisation is completed relatively early.

Observation of future 21cm experiments like LOFAR should not only provide a wealth of information on how the Universe was reionised but may also provide important clues for the growth history of supermassive black holes at very high redshift.

## ACKNOWLEDGEMENTS

The authors wish to thank Stuart Wyithe for useful comments on a draft and the referee for suggesting calculating the HII region filling factor and the degree of pre-reionisation by X-rays. KJR is supported by an Overseas Research Scholarship and the Cambridge Australia Trust. This research was supported in part by the National Science Foundation under Grant No. PHY99-07949.

## REFERENCES

- Abel, T., Anninos, P., Zhang, Y., & Norman, M. L. 1997, *New Astronomy*, 2, 181
- Barkana, R. & Loeb, A. 2001, *Phys.Rep.*, 349, 125
- Begelman, M. C., Volonteri, M., & Rees, M. J. 2006, *MNRAS*, submitted (astro-ph/0602363)
- Bolton, J., Haehnelt, M.G., 2006, *MNRAS*, submitted (astro-ph/0607331)
- Bromley, J. M., Somerville, R. S., & Fabian, A. C. 2004, *MNRAS*, 350, 456
- Chen, X. & Miralda-Escudé, J. 2004, *ApJ*, 602, 1
- Erickcek, A. L., Kamionkowski, M., Benson A. J., submitted to *MNRAS* (astro-ph/0604281)
- Fan, X., et al. 2001, *AJ*, 121, 54
- Fan, X. et al., 2002, *AJ*, 123, 1247
- Fan, X., et al. 2004, *AJ*, 128, 515
- Fan, X. et al., 2006, *AJ*, in press, astro-ph/0512082
- Ferrarese, L. 2002, *ApJ*, 578, 90
- Ferrarese, L., Merritt, D. 2000, *ApJ*, 539, L9
- Furlanetto, S.R. 2006, *MN*, submitted, astro-ph/0604040
- Gebhardt, K., et al. 2000, *ApJ*, 539, L13
- Gunn, J. E., & Peterson, B. A. 1965, *ApJ*, 142, 1633
- Haehnelt, M. G., Natarajan, P., & Rees, M. J. 1998, *MNRAS*, 300, 817
- Haiman Z., Hui L., 2001, *ApJ*, 547, 27
- Hopkins P. F., Hernquist L., Cox T. J., Di Matteo T., Martini P., Robertson B., Springel V., 2005, *ApJ*, 630, 705
- Kauffmann, G., & Haehnelt, M. 2000, *MNRAS*, 311, 576
- Kohler, K., Gnedin, N. Y., Miralda-Escudé, J., & Shaver, P. A. 2005, *ApJ*, 633, 552
- Kuhlen, M., Madau, P., Montgomery, R., *ApJ*, 2006, 637, L1
- Lacey, C., & Cole, S. 1993, *MNRAS*, 262, 627
- Madau, P., Haardt, F., & Rees, M. J. 1999, *ApJ*, 514, 648
- Madau, P., Rees, M. J., Volonteri, M., Haardt, F., Oh, S. P., 2004, *ApJ*, 604, 484
- Malhotra, S., & Rhoads, J. E., 2005, *ApJL*, submitted (astro-ph/0511196)
- Martini P., Weinberg D. H., 2001, *ApJ*, 547, 12
- Mellema, G. et al. 2006, *MNRAS*, submitted (astro-ph/0603518)
- Mesinger, A. & Haiman, Z. 2004, *ApJL*, 611, L69
- Miralda-Escudé, J., Haehnelt, M., & Rees, M. J. 2000, *ApJ*, 530, 1
- Oh, S.P., Furlanetto, S., 2005, *ApJ*, 620, L9
- Press, W. H., & Schechter, P. 1974, *ApJ*, 187, 425
- Ricotti, M., & Ostriker, J. P. 2004, *MNRAS*, 352, 547
- Scott, D., & Rees, M. J. 1990, *MNRAS*, 247, 510
- Sheth, R. K., & Tormen, G. 1999, *MNRAS*, 308, 119

- Silk, J., & Rees, M. J. 1998, *A&A*, 331, L1  
Shull, J. M., & van Steenberg, M. E. 1985, *ApJ*, 298, 268  
Spergel, D. N. et al. 2006, *ApJ*, submitted (astro-ph/0603449)  
Songaila A., 2004, *AJ*, 127, 2598  
Tozzi, P., Madau, P., Meiksin, A., & Rees, M. J. 2000, *ApJ*, 528, 597  
Volonteri, M., Haardt, F., & Madau, P. 2003, *ApJ*, 582, 559  
Wyithe, J. S. B., & Loeb, A. 2003, *ApJ*, 595, 614  
Wyithe, J. S. B. & Loeb, A. 2004a, *Nature*, 427, 815  
Wyithe, J. S. B. & Loeb, A. 2004b, *ApJ*, 610, 117  
Wyithe, J. S. B., Loeb, A., & Barnes, D. G. 2005, *ApJ*, 634, 715  
Yu, Q. 2005, *ApJ*, 623, 683  
Yu, Q., & Lu, Y. 2005, *ApJ*, 620, 31  
Yu, Q., & Tremaine, S. 2002, *MNRAS*, 335, 965  
Zaroubi, S., & Silk, J. 2005, *MNRAS*, 360, L64

This paper has been typeset from a  $\text{\TeX}$ / $\text{\LaTeX}$  file prepared by the author.